Table 1 The current expected to produce explosive boiling in a spraying liquid cone

	r_A (Å)	ρ $\left(\frac{\text{gm}}{\text{cc}}\right)$	σ $\left(\frac{\text{dyne}}{\text{cm}}\right)$	K $\frac{\text{watts}}{\text{cm K}}$	$R\times10^6$ (Ω – cm)	i_{crit} (μA)
Salt water	1.45	1.0	70	0.006	1000	-
Hg	1.55	13.6	467	0.075	98.5	46.7
Na	1.86	0.92	200	0.8	10.2	403
Cs	2.62	1.87	70	0.19	36.6	112
K	2.31	0.87	411	0.48	13	757
Cu	1.28	8.9	1100	1.75	22	549

much higher temperature than in a large bulk. Farther back from the tip, as the volume increases, the boiling temperature drops to the bulk value of approximately 0.9 T_c,[3] where T_c is the absolute critical temperature of the liquid. From the figure, it is clear that the lowest temperature for boiling will occur near the tip of the cone. Also, the temperature in a spraying cone tends to be highest at the tip, as pointed out in a previous paper. For both of these reasons we would expect the discharge to begin with the smallest particles, namely ions. As the temperature is raised, large pieces of the tip can be severed by the formation of vapor nuclei, and the discharge will then contain dimers and trimers in addition to the ions. The sequence is often observed in practice, as monomers and then dimers and large particles are emitted as the current increases. The transition from monomers to dimers would be expected when the temperature reached the explosive boiling point several atomic radii from the tip. From the geometry of the cone it is clear that this distance will be approximately $2r_A$-$3r_A$, where r_A is the atomic radius.

The discharge current at which the transition to dimer spraying occurs can be estimated by calculating the current needed to produce the boiling temperature at the critical distance from the tip, using the results of Ref. 2. The required currents, shown in Table 1, were calculated for several of the liquids of interest in electrohydrodynamic spraying, using an assumed radius of 2.5 r_A. The values for thermal conductivity K and electrical resistivity R were taken from Ref. 2.

V. Implications for the Selection of Spraying Liquids

Explosive boiling sets a limit on the maximum current and hence power that can developed in electric spraying without the formation of larger fluid particles than ions. If this limit is to be extended, liquids must be selected to lower the rate of formation of critical vapor nuclei. This rate depends chiefly on the exponential term,

$$\exp-(4\pi\sigma r_c^2/3kT) \tag{5}$$

To keep this term low, the surface tension should be high, since this increases the energy threshold for the formation of vapor nuclei. The atomic radius should be large, since this requires the formation of a larger bubble to split off the tip of the cone, and this too increases the activation energy for the transition.

The temperature of the cone should be kept as low as possible to keep the thermal energy low. From the results of Ref. 2, the temperature depends most strongly on the ratio of material properties R/K, where R is the electrical resistivity and K is the thermal conductivity. To keep the temperature low, the liquid chosen should be a good conductor of both heat and electricity.

Liquid metals obviously are good candidates for this application, with large surface tensions, thermal conductivities, and electrical conductivities. In fact, all the successful ion beams produced so far have employed liquid metals or alloys such as NaK, Cs, and GaIn. There are still many liquid metals that have not been tried, however, and the search for superior spray liquids may well begin with liquid metals with higher conductivities and surface tension than those used so far. Copper, for example, has a critical current higher than most of the other liquids listed in the table, but has not yet been tried, to the author's knowledge. Other, more exotic metals and alloys may occur to the interested reader.

References

[1]Taylor, G. I., "Disintegration of Water Drops in an Electric Field," *Proceedings of the Royal Society (London)*, Vol. A280, 1964, p. 383.

[2]Crowley, J. M., "Role of Joule Heating in the Electrostatic Spraying of Liquids," *Journal of Applied Physics*, Vol. 48, 1977, p. 145.

[3]Cole, R., "Boiling Nucleation," *Advances in Heat Transfer*, Vol. 10, 1974, p. 85.

[4]Reid, R. C., "Superheated Liquids," *American Scientist*, Vol. 64, 1976, p. 146.

Parabolic-Series Method for Transonic Wedge Flow

D. D. Liu*
Northrop Corporation, Hawthorne, Calif.

Introduction

LIU and Platzer[1] have recently developed two related approximate methods for transonic wedge flow calculation in which the flowfield decay in the lateral direction is prescribed, a priori, by some analytical functions. Both methods yield reasonably good results in comparison with the exact theory[2] and the method of local linearization.[3] The purpose of this Note is to present an improvement of the results obtained in Ref. 1, by employing a parabolic-decay series. Also, we begin with a more general formulation than that in Ref. 1, yielding equations accounting for the effects of flowfield correction and surface curvature.

Unlike the source-distribution methods for the linear theory, the methods in Ref. 1 aim at solving the approximate nonlinear structure of the near field in the proximity of the body surface. Thus, method A is essentially an integral method similar to the Karman-Pohlhausen approach to the boundary-layer problem; method B directly solves the asymptotic equation which is related to the so-called method of series truncation.[4] The difference between the latter two methods is that in method B, the problem of closure (the number of unknown functions exceeds the number of equations) is curcumvented by introducing a known decaying function, a priori, whose dependent variable is a stretched parabolic coordinate η in the lateral direction. Two decaying functions have been adopted to depict the decay of the flow disturbance: namely, an algebraic decaying function and an exponential decaying function, i.e.

$$F(\eta)=1/(1+\eta)^{\alpha} \quad , \quad \alpha>1/2 \tag{1a}$$

$$F(\eta)=e^{-\lambda\eta} \quad , \quad \lambda>0 \tag{1b}$$

(See Eqs. 2.13(a) and 2.13(b) of Ref. 1.)

It was concluded that the choice of these decaying functions really does not affect the basic form of the solution and hence the pressure behavior. But the drag coefficient is much more sensitive to whichever of these functions is chosen. For this reason, we have investigated a number of other possible forms of the decaying functions. The decaying function extracted

Received Nov. 29, 1976; revision received Feb. 16, 1977.
Index categories: Aerodynamics; Subsonic and Transonic Flow.
*Engineering Specialist. Member AIAA.

from the parabolic method[5] then appears to be a promising candidate; interestingly, it turns out to give excellent results both in the pressure distribution and the drag coefficient.

In the subsequent development, dimensionless variables are introduced as: $x=\bar{x}/L, y=\tau^{1/3}\bar{y}/L$, and $\varphi(x,y)=\tau^{-2/3}\bar{\varphi}(\bar{x},\bar{y})$; where L is the characteristic length chord), τ is the body thickness ratio, and barred symbols denote the true physical quantities.

Formulation

The transonic small perturbation equation ($M_\infty=1$) can be generally expressed in a compact form for parabolic approximation ($\sigma=0$) and the nonlinear form ($\sigma=1$) as

$$\varphi_{yy}=\Lambda_\sigma[(1-\sigma)\varphi+\sigma\varphi_x{}^2] \tag{2}$$

where

$$\Lambda_0=K\frac{\partial}{\partial x}, \quad K=\text{parabolic constant} \tag{2a}$$

$$\Lambda_1=\frac{\gamma+1}{2}\frac{\partial}{\partial x}, \quad \gamma=\text{specific heat ratio of the gas} \tag{2b}$$

Following Hosokawa,[6] the parabolic solutions for $\sigma=0$ [Eq. (2a)] can be written in a series form as

$$\varphi(\xi,\eta)=-\frac{1}{2\sqrt{\pi}}\sum_{n=0}^{N}X_n(\xi)H_n(\eta) \tag{3}$$

where

$$X_n(\xi)=f^{(n+1)}(\xi)\cdot\xi^{n+1/2} \tag{3a}$$

$$H_n(\eta)=J_{n+1}(\eta)\cdot\eta^{2n+1} \tag{3b}$$

and N is some positive integer.

Equation (3) is based on a coordinate transformation (ξ,η) defined as

$$\xi=x \quad , \quad \eta=y\cdot g(x) \tag{3c}$$

where $g(x)$ is the stretching function. In the sense of parabolic solution, $g(x)$ is identified to be $(K/4x)^{1/2}$.

The function $f^{(n+1)}(\xi)$ is defined as $\mathrm{d}^{n+1}f(\xi)/\mathrm{d}\xi^{n+1}$ and $f(\xi)$ is the source distribution function related to the profile slope, while the parabolic decaying function $J_{n+1}(\eta)$ is defined as

$$\left\{\begin{aligned} J_{n+1}(\eta)&=\frac{2^{2(n+1)}(n+1)!}{[2(n+1)]!}\left\{\sum_{k=0}^{n}(-1)^k\frac{[2(n-k)]!}{(n-k)!2^{2(n-k)+1}}\right.\\ &\left.\cdot\frac{e^{-\eta^2}}{\eta^{2(n-k)+1}}+(-1)^{n+1}J_0(\eta)\right\} \qquad (3d)\\ J_0(\eta)&=\int_\eta^\infty e^{-u^2}\mathrm{d}u \qquad (3e)\end{aligned}\right.$$

On the other hand, the nonlinear equation (2b) ($\sigma=1$), under the transformation (3c), becomes

$$\begin{aligned}&(\gamma+1)[\varphi_\xi+G_0(\xi)\cdot\eta\varphi_\eta]\cdot[\varphi_{\xi\xi}+G_0{}^2(\xi)\eta^2\varphi_{\eta\eta}\\ &+2G_0(\xi)\eta\varphi_{\eta\xi}+G_1(\xi)\eta\varphi_\eta]=g^2(\xi)\cdot\varphi_{\eta\eta}\end{aligned} \tag{4}$$

where

$$G_0(\xi)=g'(\xi)/g(\xi)$$

$$G_1(\xi)=g''(\xi)/g(\xi)$$

In the present case, $g(\xi)$ shall be related to the profile slope $h'(\xi)$ by the tangency condition [see Eq. (2.5), Ref. 1].

Following our previous approach in Ref. 1, we seek the nonlinear potential solution in the "separable" form of

$$\varphi(\xi,\eta)\simeq\sum_{n=0}^{N}U_n(\xi)H_n(\eta) \tag{5}$$

Clearly, $H_n(\eta)$ is the parabolic decaying function extracted from the linearized parabolic solution which satisfies the farfield conditions required for φ and its derivatives. Notice that the source distribution functions $X_n(\xi)$ are now replaced by the unknown functions $U_n(\xi)$, which are to be sought in the following development.

To demonstrate the procedure, we take three terms in Eq. (5) (i.e., $N=2$) and substitute them into Eq. (4). In accordance with the order of η^0, η^1, and η^2, respectively, we obtain

$$(\gamma+1)\cdot\phi_0'\phi_0''=2g^2\phi_2 \tag{6a}$$

$$(\gamma+1)\cdot[\phi_1'+G_0\phi_1)\phi_0''+(\phi_1''+2G_0\phi_1'+G_1\phi_1)\phi_0']=6g^2\phi_3 \tag{6b}$$

$$\begin{aligned}&(\gamma+1)\cdot[(\phi_2'+2G_0\phi_2)\phi_0''+(\phi_1'+G_0\phi_1)(\phi_1''+2G_0\phi_1'\\ &+G_1\phi_1)+(\phi_2''+4G_0\phi_2'+2G_0{}^2\phi_2+2G_1\phi_2)\phi_0']=12g^2\phi_4\end{aligned} \tag{6c}$$

where

$$\phi_0(\xi)=U_0+\frac{1}{3}U_1+\frac{1}{5}U_2 \tag{6d$_1$}$$

$$\phi_1(\xi)=-\sqrt{\pi}U_0 \tag{6d$_2$}$$

$$\phi_2(\xi)=U_0-U_1-\frac{1}{3}U_2 \tag{6d$_3$}$$

$$\phi_3(\xi)=\frac{2\sqrt{\pi}}{3}U_1$$

$$\phi_4(\xi)=-\frac{1}{6}U_0-\frac{1}{2}U_1+\frac{1}{2}U_2 \tag{6d$_4$}$$

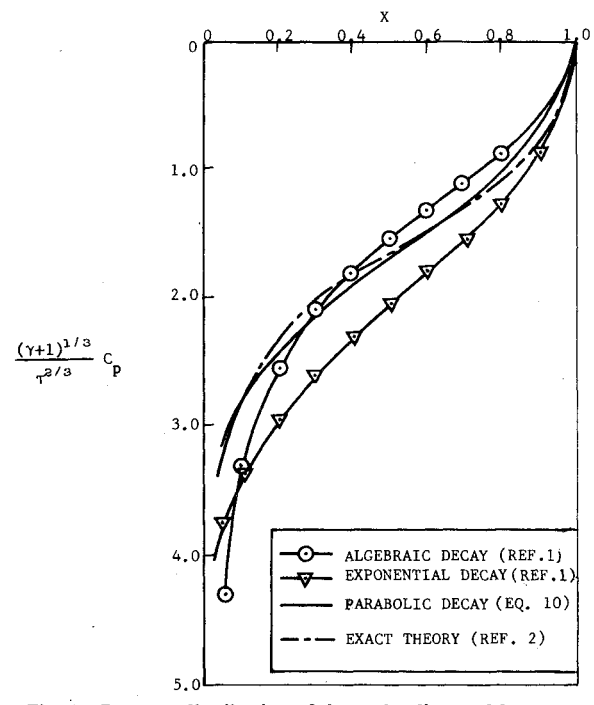

Fig. 1 Pressure distribution of the wedge flow at $M_\infty=1.0$.

Based on the tangency condition, $g(\xi)$ can now be expressed as

$$g(\xi)=h'(\xi)/\phi_1(\xi) \tag{7}$$

Inserting Eq. (7) into Eqs. (6a and 6b) results in

$$(\gamma+1)\phi_1^2\phi_0'\phi_0''=2h'^2\phi_2 \tag{8a}$$

$$(\gamma+1)\phi_1^3[h'''\phi_0'+h''\phi_0'']=6h'^3\phi_3 \tag{8b}$$

$$\text{Eq. (6c)}+\text{Eq. (7)} \tag{8c}$$

As the combined form of Eqs. (7) and (6c) [labeled as Eq. (8c)] is rather lengthy; it shall not be given here. It is apparent that for the case of the wedge, h'' and h''' are both zero in Eq. (8b), which leads to $U_1(\xi)=0$. However, if we carry out Eq. (8c) and drop all terms involving h'' and h''', the following equation results

$$(\gamma+1)[\phi_0''(\phi_1^2\phi_2'-2\phi_1\phi_1'\phi_2)+\phi_0'(\phi_1^2\phi_2''$$
$$-4\phi_1\phi_1'\phi_2'+6\phi_1\phi_1'^2\phi_2-2\phi_1\phi_1''\phi_2)]=12h'^2\phi_4 \tag{8d}$$

Clearly, Eqs. (8a) and (8d), containing only two unknown functions, $U_0(\xi)$ and $U_2(\xi)$, are thus consistent equations obtained up to the order of η^2. They are to be solved simultaneously, in principle, subject to the following conditions

$$\begin{cases} U_0(0)=U_2(0)=0 & \text{at the apex} \quad (9a) \\ U_0'(1)=U_2'(1)=0 & \text{at the shoulder} \quad (9b) \end{cases}$$

Wedge-Flow Analysis

Instead of solving Eqs. (8a) and (8d) as a simultaneous set, alternatively, the approximate scheme according to the principle of series truncation method[4] is to solve Eq. (8a) itself alone and to impose $U_2=0$. In this way, the approximate scheme proposed can be considered as a first step toward an iterative scheme and the subsequent solution of $U_2(\xi)$ of Eq. (8d) can be considered as a flowfield correction to $U_0(\xi)$ of Eq. (8a). In what follows, however, we only restrict the analysis to the solution of Eq. (8a), as our purpose is to elucidate the improvement made due to the usage of the parabolic decaying function.

The explicit form of Eq. (8a) reads

$$U_0U_0'U_0''=B, \quad B=2/\pi(\gamma+1) \tag{10}$$

whose boundary conditions are given in Eq. (9). An exact solution has been given in Ref. 1 in an implicit form [Eq. (4.4)], i.e.

$$\xi=\frac{1}{\Gamma(2/3)}\int_0^{\bar{U}_0}\frac{d\mu}{|\ln\mu|^{1/3}} \tag{11}$$

where $0\le\xi\le1$ and $0\le\bar{U}_0=\dfrac{U_0(\xi)}{U_0(1)}\le1$

$$\Gamma(2/3)=1.35411794...$$

the Gamma function. Meanwhile, Eq. (10) can be integrated to yield a first order equation, i.e.,

$$U_0'(\xi)=-(3B)^{1/3}|\ln\bar{U}_0|^{1/3} \tag{12}$$

The pressure coefficient $C_p=-2\tau^{2/3}\varphi_x(x,0)$ can now be expressed as

$$\bar{C}_p=\frac{(\gamma+1)^{1/3}}{\tau^{2/3}}C_p=2\left(\frac{6}{\pi}\right)^{1/3}|\ln\bar{U}_0|^{1/3} \tag{13}$$

Thus, the drag coefficient defined as $C_D=\tau\int_0^1 h'(x)\,C_p\,dx$ can be derived as

$$\bar{C}_D=\frac{(\gamma+1)^{1/3}}{\tau^{5/3}}C_D=\frac{2(6/\pi)^{1/3}}{\Gamma(2/3)}\simeq1.83 \tag{14}$$

Hence, the present drag results is considered to be an improvement over our previous result $\bar{C}_D=1.9$ according to the algebraic decaying function ($\alpha=1$). In order to compare with the exact value of Guderley-Yoshihara[2] and other approximate hodograph methods, the following results are quoted: $\bar{C}_D=1.67$ (Cole[7]); $\bar{C}_D=1.75$ (Guderley-Yoshihara[2]); $\bar{C}_D\simeq1.89$ (others in Ref. 8).

The pressure coefficient is obtained by numerical integration of Eq. (11). It can be seen in Fig. 1, that the present parabolic decaying function indeed gives better agreement with the exact theory than those functions proposed in Ref. 1. Also, when we apply the iteration scheme proposed in Ref. 1 by substituting the parabolic solution for a wedge into the right-hand side of Eq. (12), the following pressure coefficient is obtained, i.e.

$$\bar{C}_P=2(3/\pi)^{1/3}|\ln\xi|^{1/3}$$

Thus, we have recovered Spreiter's wedge solution[3] from a rather different approach.

Discussion

By contrast, the present approach is different from the parabolic method and the local linearization method in the sense that no free constant is required to be determined nor is it needed to be reset into a variable. Neither the parabolic method nor Hosokawa's method is known to be adequate for the wedge flow calculation, since those models break down as the flow approaches the wedge shoulder. We have shown that, on the other hand, the present method adopting the parabolic-decay series indeed gives excellent results both in the drag coefficient and the pressure distribution in comparison with the exact theory; the iteration version of the present method recovers the local linearization result as a special case. Furthermore, we have drived a higher-order flowfield correction scheme [Eqs. (8a) and (8d)], which is an improvement over the previous approach.[1] Hence, the present approach would amount to the possible extension of the lifting and unsteady cases of the wedge flow. Within the framework of the present formulation, it is believed that the axisymmetric case for a transonic cone flow can also be solved in the same manner. Some difficulties, however, are expected in tackling the profiles with curvatures (such as parabolic arc airfoil), due to the fact that the sonic-point location is unknown in advance.

Acknowledgment

The author would like to thank R. E. Singleton of the Army Research Office, Durham, North Carolina, and M. F. Platzer of the Naval Postgraduate School, Monterey, California, for valuable discussions. The suggestions made by R. Schamberg on the manuscript, and the checking of the algebra rendered by P. A. Hill of Northrop Corporation were most helpful.

References

[1] Liu, D. D. and Platzer, M. F., "Approximate Methods for Transonic Flow Past Finite Wedge Profiles," *Zeitschrift für Angewandte Mathematik und Mechanik*, 56, Jan. 1976, pp. 51-57.

[2] Guderley, K. and Yoshihara, H., "The Flow Over a Wedge Profile at Mach Number 1," *Journal of the Aeronautical Sciences*, Vol. 17, Nov. 1950, pp. 723-735.

[3] Spreiter, J. and Alksne, A., "Thin Airfoil Theory Based on Approximate Solution of the Transonic Flow Equation," NACA TR1359, 1958.

[4] Van Dyke, M. D., "A Method of Series Truncation Applied to Some Problems in Fluid Mechanics," *Fluid Dynamics Transactions*, Vol. 3, Friszdon, et al., Editors, Warsaw, 1967, pp. 53-67.

[5]Oswatitsch, K. and Keune, F., "Flow Around Bodies of Revolution at Mach Number One," *Proceedings of the Conference on High Speed Aerodynamics*, Polytech. Inst. of Brooklyn, 1955, pp. 113-131.

[6]Hosokawa, I., "A Refinement of the Linearized Transonic Flow Theory," *Journal of the Physical Society of Japan*, Vol. 15, No. 11, 1960, pp. 149-157.

[7]Cole, J. D., "Drag of the Finite Wedge at High Subsonic Speeds," *Journal of Mathematics and Physics*, Vol. 30, No. 2, July 1951, pp. 79-93.

[8]Ferrai, C. and Tricomi, F., *Transonic Aerodynamics*, Academic Press, New York, 1968, pp. 231-260.

Shock-Wave Profiles about Hemispherical Noses at Low Supersonic Mach Numbers

K. D. Korkan* and G. M. Gregorek†
Ohio State University, Ohio

In a recent Synoptic, Hsieh[1] presented the results of a systematic theoretical and experimental study of a hemisphere-cylinder at zero incidence for Mach numbers ranging from 0.7 to 2. In the computational segment of the analysis, a direct method of a time-dependent finite difference solution to the unsteady Euler's equation is employed. As a result, Hsieh was able to present comparisons of theoretical shock positions about a hemispherical nose with existing and obtained experimental data.

It is interesting to note that a correlation concept of the bow shock profile for spheres utilizing the density ratio across a normal shock was employed by Gregorek and Korkan[2] in a study of hypersonic blunt body similitude. In this study,[2] the general form of the equation for the spherical shock as obtained from the blast wave analogy was employed, i.e.

$$r_s/d_N = A\ [x/d_N]^n \tag{1}$$

where the coordinate system is taken at the origin of shock apex. As reported in Ref. 3, shock wave profile experimental data were obtained in the 4-in. continuous, free-jet, hypersonic wind tunnel of the Ohio State University. Values of the shock wave radial coordinate r_s and the axial coordinate x were thus determined. When these values were nondimensionalized by the sphere diameter d_N and displayed on a logarithmic scale, the profiles were observed to be approximately linear and therefore could be expressed in the form of Eq. (1). However, the correlations presented earlier[2,3] were based upon $M_\infty \geq 2$ data. With the data exhibited by Hsieh,[1] these correlations may now be extended to the low supersonic Mach numbers.

Employing the shock wave constants obtained for spheres,[2] in addition to Hsieh,[1] Seiff,[4] Baer,[5] and Love,[6] values for A and n were plotted against Mach number as shown in Fig. 1 for $\gamma = 1.4$. From these results, the empirical correlation for A and n based on a density ratio presented earlier[2] has been modified to fit the experimental data and takes the form

$$A = 1.52\ k^{-0.20} + [0.823/(M_\infty^2 - 1)] \tag{2}$$

$$n = 0.61\ M_\infty^{-0.11} \tag{3}$$

Received Nov. 29, 1976; revision received Feb. 14, 1977.
Index categories: Shock Waves and Detonations; Supersonic and Hypersonic Flow.

*Research Associate, Department of Aeronautical and Astronautical Engineering. Associate Fellow AIAA.
†Professor, Department of Aeronautical and Astronautical Engineering. Member AIAA.

and therefore Eq. (1) becomes

$$\frac{r_s}{d_N} = \left[1.52\ k^{-0.20} + \frac{0.823}{(M_\infty^2 - 1)}\right]\left(\frac{x}{d_N}\right)^{0.61 M_\infty^{-0.11}} \tag{4}$$

The experimental values of A are well represented by their empirical expression, with the maximum deviation being less than 2%. Values of the exponent n show more scatter, due to the greater measurement difficulty in obtaining the slope of the shock wave profile from the experimental data.

Application of the present empirical correlation expressed in Eq. (4) to the experimental results shown by Hsieh[1] and Gregorek and Korkan[2] is presented in Fig. 2. As can be seen, the agreement between prediction and experiment is acceptable over a wide range of Mach numbers which now encompass the low supersonic regime, e.g., $12.00 \geq M_\infty \geq 1.10$. It may also be noted that the results of Figs. 1 and 2 may be plotted in terms of density ratio across a normal shock k as had been done earlier[2] with good agreement with experimental data for $k \leq 15$.

Since the empirical correlation given by Eq. (4) has a coordinate system located at the apex of the shock wave profile, the shock detachment distance has also been investigated. Using the data presented by Hsieh[1,7-10] and those given by Gregorek and Korkan,[2,5,11] a comparison has been made with the shock detachment distance prediction utilizing the Ambrosio and Wortman[11] expression based on k, i.e.

$$\Delta/r_N = 0.52\ (k-1)^{-0.861} \tag{5}$$

The results are shown in Fig. 3 and indicate good agreement between Eq. (5) and experiment over a wide range of Mach numbers including the low supersonic regime, i.e., $15.00 \geq M_\infty \geq 1.10$.

Therefore, with the aid of the data presented by Hsieh[1] and other investigators, the empirical correlation[2,3] based on k and M_∞ to predict the shock wave profile about a hemispherical nose has been extended to include Mach numbers ≥ 1.10 while still being valid up to $M_\infty \simeq 15$. It has also been shown that the shock detachment distance for a hemispherical nose can also be predicted up to $M_\infty \simeq 15$ including the low supersonic range by an empirical expression originally formed by Ambrosio and Wortman.[11] The expressions presented by Eqs. (4) and (5) provide a rapid method to predict the shock wave profile and detachment distance about a hemispherical nose for $15.00 \geq M_\infty \geq 1.10$. However, the need for computational methods still exists to satisfy such requirements as obtaining the details of the

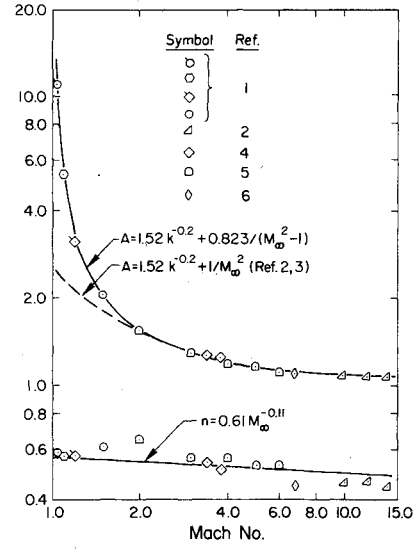

Fig. 1 Dependence of shock wave constants on freestream Mach number.